



# Modulation of spin-orbit torque efficiency by thickness control of heavy metal layers in Co/Pt multilayers



P. Sethi, S. Krishnia, S.H. Li, W.S. Lew\*

School of Physical & Mathematical Sciences, Nanyang Technological University, 21 Nanyang Link, 637371, Singapore

## ARTICLE INFO

### Keywords:

Spin orbit torque  
Spin Hall angle  
Perpendicular magnetic anisotropy

## ABSTRACT

We investigate and quantify spin-orbit torque (SOT) strength by current induced effective in-plane magnetic fields and spin Hall angle (SHA) using AC harmonic Hall voltage measurements techniques on Ta/Pt/Co/Pt/Co/Ta thin film structures. The proposed Co/Pt thin film double stack gives property enhancement on thermal stability and perpendicular magnetization anisotropy strength over the single stack Pt/Co/Ta. In the proposed Co/Pt double stack we observed that increasing the Ta capping thickness to three times enhances the SHA in similar order, consistent with larger spin injection efficiency. Doubling the Pt spacer layer thickness reduces the SHA by nearly 1.4 times, due to partial cancellation of SOT by bottom layer Pt, negating the increase from the top Co/Pt interface. The in-plane current threshold for magnetization switching is lower with the increase of the SHA.

## 1. Introduction

Efficient magnetization switching is crucial for realizing state-of-the-art, high speed and reliable non-volatile memory and logic devices [1–4]. Conventional methods that rely on spin-transfer torque (STT) technique [5,6] have limitations as they require materials to spin polarize the current or ferromagnets with specific spin textures. More recently spin-orbit torque (SOT) has emerged as the preferred mode of magnetization switching [7–9] and domain wall driving mechanism [10–13]. SOT switching, which does not require materials to polarize the current, can arise in systems with strong spin-orbit coupling and inversion asymmetry through the Rashba effect [7] and the spin Hall effect (SHE) [8,9]. In STT, whereas the spin transfer limits the maximum torque efficiency by the total amount of spin polarization, there is no such limitation in materials with strong spin-orbit coupling [14]. The commercial application of spin transfer which is STT-MRAM suffers from tunnel oxide degradation due to high write currents. SOT based MRAM separates the read and write paths and hence increases the device endurance. Thus SOT finds applications in devices like magnetic tunnel junctions [15], spin logic [16] and magnetic random number generator [17]. The current induced effective fields, which are manifestations of the SHE and Rashba effects, are direct measures of the SOT strength [18,19]. Spin Hall angle (SHA), which is the ratio of spin current to the charge current, can be computed from the effective field values and is used to quantify the effect due to SOT. Pt and Ta have been extensively studied as underlayer and capping layers due to

their relatively large SHA, 0.07 and  $-0.12$ , respectively. Recent work has focussed on exploring alternative metals possessing larger SHA, for instance beta phase of W with record SHA of 0.31 [20]. Numerous studies have been carried out to tune the SHA by varying the thickness of the heavy metal layers [18,19,21,22]. Most of the studies have confined to single ferromagnetic layer to obtain perpendicular magnetization anisotropy (PMA), however, at the cost of poor thermal stability which is a major obstacle for scaling down to a few nanometers. Pt/Co/Ta is known to possess enhanced SOT strength on account of opposite SHAs of Pt and Ta. The stack, however, is prone to inter-diffusion of Ta and Co thereby reducing the PMA strength [23]. We provide a solution to this issue by inserting an additional Co/Pt interface to the single stack, which enhances the thermal stability and the PMA strength. Increasing the Pt spacer thickness two times reduces the SHA by nearly 1.4 times due to partial cancellation with the underlayer Pt, increasing the Ta capping layer three times increases the SHA by nearly three times. The current induced magnetization switching efficiency increases on increasing the SHA.

## 2. Experimental results and discussion

Thin films of single and double stack Co/Pt structures were deposited on silicon dioxide coated silicon wafers. Sample A, SiO<sub>2</sub>/Ta (3)/Pt (3)/Co (0.7)/Ta (1) & Sample B, SiO<sub>2</sub>/Ta (3)/Pt (3)/Co (0.7)/Pt (0.5)/Co (0.7)/Ta (1), thicknesses are in nm, were deposited using magnetron sputtering technique at a base pressure of  $2 \times 10^{-8}$  Torr. The

\* Corresponding author.

E-mail address: [wensiang@ntu.edu.sg](mailto:wensiang@ntu.edu.sg) (W.S. Lew).

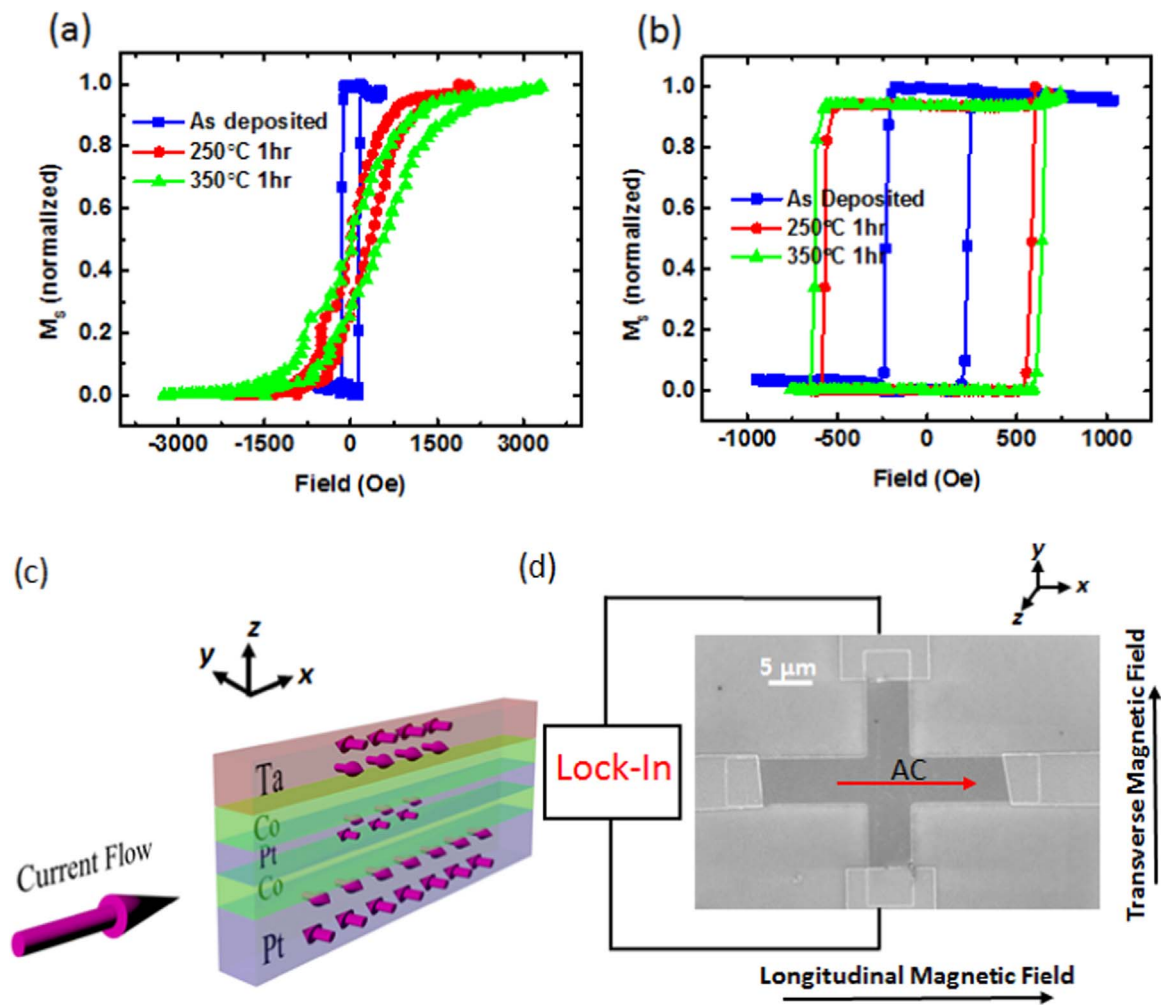


**Fig. 1.** (a) M-H loops of thin film stacks, Pt/Co/Ta measured before and after annealing. (b) M-H loops of thin film stack Ta/Pt/Co/Pt/Co/Ta measured before and after annealing. (c) Schematic depicting the Co/Pt double stack, in-plane current causes the respective spin current distribution in the heavy-metal layers; the sign of the spin depends on the spin Hall angle and the spin density depends on the thickness. (d) Scanning electron microscopy image of the fabricated Hall cross structure; the schematic depicts set-up for AC harmonic measurements.

M-H curves were measured for the two as-deposited thin films using magneto optical Kerr effect (MOKE) technique. To compare the thermal stabilities of the two stacks, the films were annealed in vacuum at 250 °C & 350 °C for 1 h and the M-H curves were again measured post annealing. The maximum annealing temperature was chosen as 350 °C to check for CMOS processing compatibility. Fig. 1(a) shows the M-H curves for sample A before and after annealing. The as-deposited sample exhibits square hysteresis with a coercivity of 100 Oe on sweeping the out-of-plane magnetic field. As the sample is annealed to 250 °C the sample loses perpendicular anisotropy as indicated by the M-H curve, further annealing to 350 °C causes little change in the M-H loops. Fig. 1(b) shows the M-H curves for sample B before and after annealing. Sample B has a coercivity of 250 Oe before annealing which increases to 500 Oe upon annealing to 250 °C and the squareness of the hysteresis is maintained, further annealing to 350 °C leads to very little change in the magnetization. The above results indicate that single stack Co/Pt is not thermally stable and has lesser PMA strength than the double stack Co/Pt. The degradation of PMA could be due to interdiffusion of Ta into Co as was proposed previously by Woo et al. through their x-ray photoelectron spectroscopy (XPS) data [23]. It is worth noting that the stack proposed by Woo et al., consisted of TaO<sub>x</sub> capping to break the inversion symmetry as opposed to our stack. There is lack of evidence to suggest that the presence of TaO<sub>x</sub> would enhance the SOT strength since it is not in direct contact with the ferromagnetic layer, unless the oxygen diffuses to the ferromagnetic

layer [24]. The XPS results in fact, indicated a reduction in oxygen intermixing with Co with increase in Ta layer thickness and increase in the Ta layer thickness exhibited enhanced SOT in the stack proposed by Woo et al. Even though the Co and Ta intermixing would be limited in our stack, we cannot ignore the possibility of Co and Pt intermixing in the stack. However, recent report suggests no significant change in the magnetic quality or PMA degradation due to Co and Pt intermixing [25].

The ferromagnetic layer in Co/Pt double stack with Ta capping experiences SOT from the heavy metal layers on account of spin-orbit coupling and structural inversion asymmetry. Fig. 1(c) shows a schematic depicting spin current distribution in the heavy metal layers of the stack under consideration due to SHE when an in-plane current is passed. The distribution takes into account the signs of spin Hall angles of Pt and Ta which are positive and negative, respectively. The spin density is proportional to the heavy metal layer thickness, with thicker heavy metal layer carrying more spin current. The bottom ferromagnetic layer, Co, experiences a net Slonczewski-like (SL) torque along the  $-y$ -direction since the bottom Pt layer is thicker as compared to the spacer Pt layer. The top Co layer would also experience net SL torque along the  $-y$ -direction as the contribution from Ta and Pt layer would add up in this case. The combination of above two contributions would give rise to a net SL torque along the  $-y$ -direction. It should be taken into consideration that the double Co/Pt stack would have lesser enhancement in SOT as compared to single stack Co/Pt due to partial

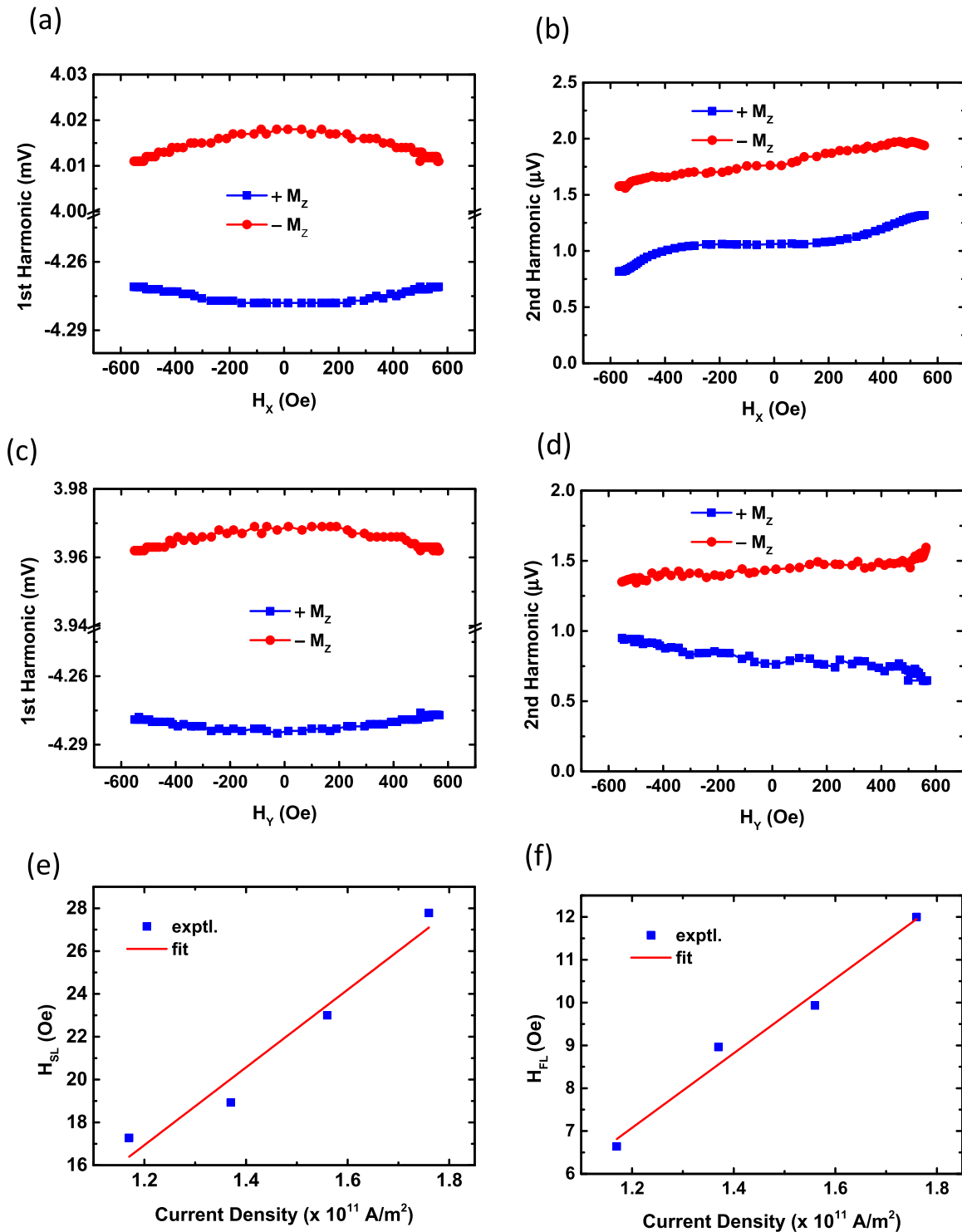


**Fig. 2.** Harmonic measurements: Ta capping thickness=1 nm, Pt spacer thickness=0.5 nm (a) 1st harmonic and (b) 2nd harmonic on sweeping longitudinal field. (c) 1st harmonic and (d) 2nd harmonic on sweeping transverse field. Effective field variation with AC density are shown in (e) for  $H_{SL}$  and (f) for  $H_{FL}$ .

cancellation of the torques from the Pt spacer layer.

Harmonic Hall voltage measurements were performed on Co/Pt double stack to estimate the effective longitudinal and transverse fields generated due to the SOT from the heavy metals [18,26–28]. The Co/Pt double stack was patterned into 5  $\mu\text{m}$  wide Hall cross structures using electron beam lithography and Ar-ion milling techniques for measuring the effective field strengths. Fig. 1(d) shows the scanning electron microscopy image (SEM) of the fabricated device and the measurement set-up for performing AC harmonic Hall voltage measurements. An

alternating current of fixed amplitude and frequency was applied across the micron-sized wire, causing the out-of-plane component of the magnetization,  $M_z$ , to oscillate at the driving frequency,  $\omega$ . The in-phase first harmonic,  $V_\omega$  and the out-of-phase second harmonic,  $V_{2\omega}$  signals were detected by measuring the anomalous Hall voltages across the Hall probe using a lock-in amplifier. The measurements were performed while sweeping either a longitudinal field  $H_L$  or a transverse field  $H_T$  to obtain Slonczewski-like effective field,  $H_{SL}$  or field-like effective field  $H_{FL}$ , respectively, using the following relation [18]:

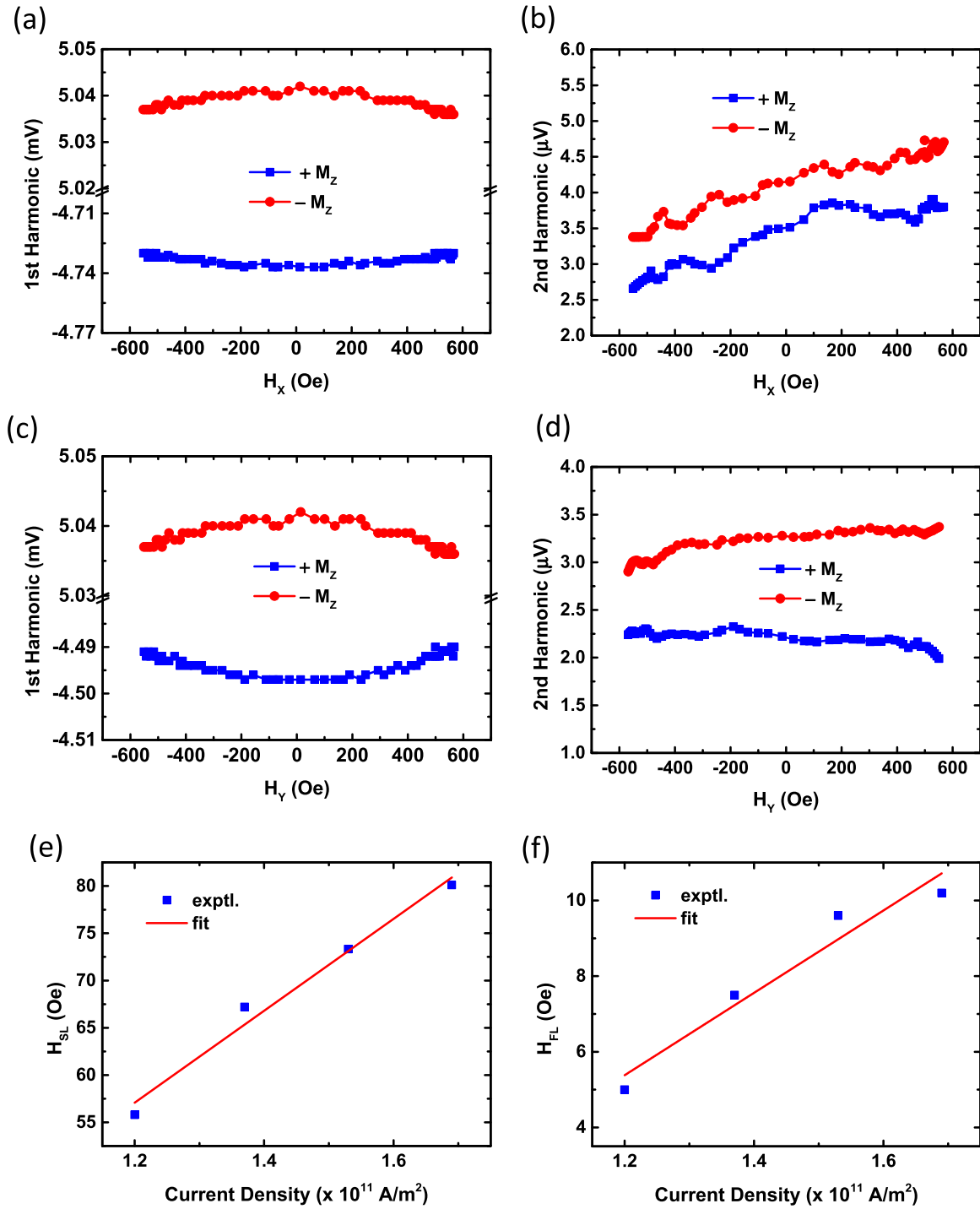


**Fig. 3.** Harmonic measurements: Ta capping thickness=3 nm, Pt spacer thickness=0.5 nm (a) 1st harmonic and (b) 2nd harmonic on sweeping longitudinal field. (c) 1st harmonic and (d) 2nd harmonic on sweeping transverse field. Effective field variation with AC density are shown in (e) for  $H_{SL}$  and (f) for  $H_{FL}$ .

$$H_{SL(FL)} = -2 \left( \frac{dV_{2\omega}}{dH_{L(T)}} \right) / \left( \frac{d^2V_{\omega}}{dH_{L(T)}^2} \right) \quad (1)$$

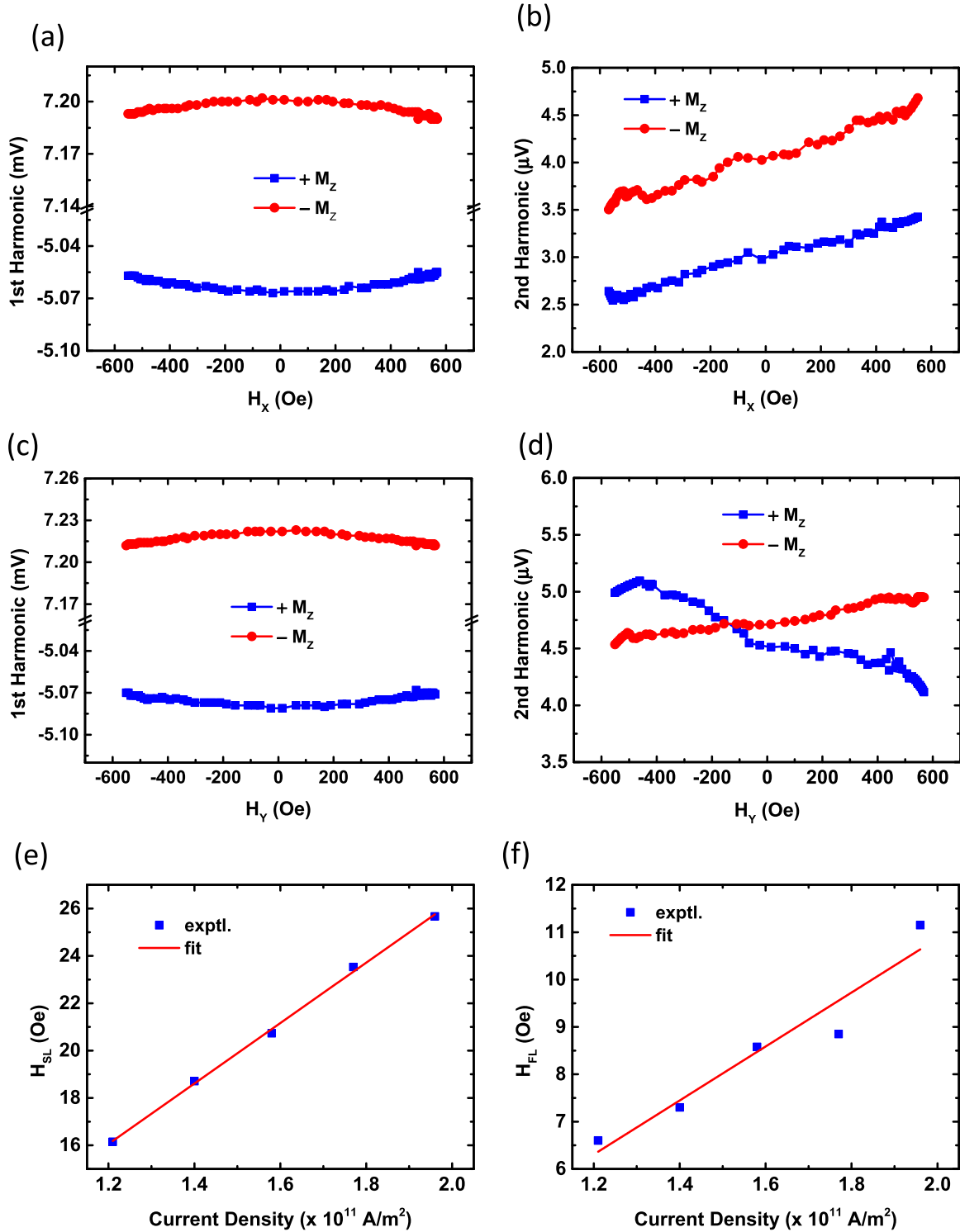
The above equation defines effective fields in terms of the direction of current flow. The excitation frequency used was  $\omega/2\pi=33$  Hz with the in-plane field swept quasi-statically from  $-600$  Oe to  $+600$  Oe. The frequency was kept low to ignore the phase difference between current and effective field oscillations.

Fig. 2(a) shows  $V_{\omega}$  versus  $H_X$  ( $H_L$ ) at a current density of  $1.17 \times 10^{11}$  A/m<sup>2</sup>, measured for up and down magnetized states of the micron-wire. The curves for up and down magnetized states are similar

and symmetric with respect to the  $x$ -axis apart from their opposite signs. A polynomial fitting was performed on the parabolic curve for  $+M_z$  to obtain an equation of the form:

$$V_{\omega} = B_1 H_X + B_2 H_X^2, \quad (2)$$

where  $B_1$  and  $B_2$  are the polynomial coefficients of the fitted equation. Fig. 2(b) shows  $V_{2\omega}$  versus  $H_X$  at a current density of  $1.17 \times 10^{11}$  A/m<sup>2</sup>, measured for up and down magnetized states of the micron-wire. The curves for up and down magnetized states have the same slope and are linearly increasing but with different magnitudes. A linear fitting was performed for  $+M_z$  to obtain an equation of the form:



**Fig. 4.** (a) Harmonic measurements: Ta capping thickness=1 nm, Pt spacer thickness =1 nm (a) 1st harmonic and (b) 2nd harmonic on sweeping longitudinal field. (c) 1st harmonic and (d) 2nd harmonic on sweeping transverse field. Effective field variation with AC density are shown in (e) for  $H_{SL}$  and (f) for  $H_{FL}$ .

$$V_{2\omega} = B_0 H_x + C, \quad (3)$$

where  $B_0$  is the slope and  $C$  is the intercept of the curve. Substituting from (2) and (3) in (1) gives the following relation:

$$H_{SL} = -\frac{B_0}{B_2} \quad (4)$$

A similar relation exists for  $H_{FL}$ , when  $V_\omega$  and  $V_{2\omega}$  are measured versus  $H_y$  ( $H_T$ ). Figs. 2(c) and 2(d) show the respective plots. Variation of  $V_\omega$  with  $H_y$  has an identical trend as that of with respect to  $H_x$ .

However,  $V_{2\omega}$  versus  $H_y$  has opposite signs of slope for  $+M_z$  and  $-M_z$  initial magnetizations.

The effective fields  $H_{SL}$  and  $H_{FL}$ , estimated using Eq. (4), were plotted versus the applied alternating current density and found to vary linearly. Figs. 2(e) and (f) show the linear relation of  $H_{SL}$  and  $H_{FL}$ , respectively, with the current density.  $H_{SL}$  and  $H_{FL}$  were evaluated as 18.13 Oe per  $10^{11}$  A/m<sup>2</sup> and 8.7 Oe per  $10^{11}$  A/m<sup>2</sup>, respectively, from the slopes of the plots. The SHA ( $\theta_{sh}$ ) was estimated for the device using the relation,  $H_{SL} = \hbar\theta_{sh}j_e V / (2lelM_t t_f)$  [29], with  $t_f$  as the ferromag-

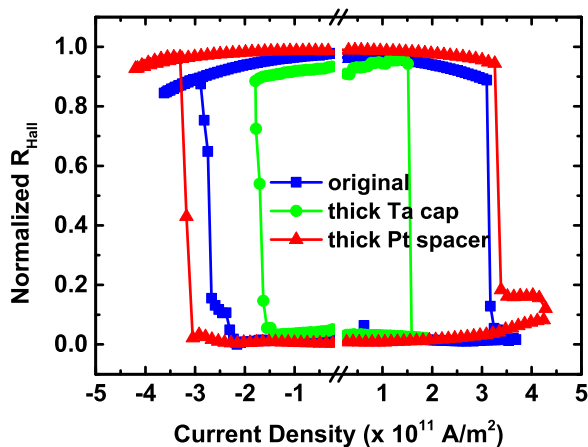


**Fig. 5.** Normalized  $R_{\text{Hall}}$  versus in-plane current density depicting magnetization switching comparison between the devices with following stack composition (i) original: Ta (3)/Pt (3)/Co (0.7)/Pt (0.5)/Co (0.7)/Ta (1); (ii) thick Ta cap: Ta (3)/Pt (3)/Co (0.7)/Pt (0.5)/Co (0.7)/Ta (3) and (iii) thick Pt spacer: Ta (3)/Pt (3)/Co (0.7)/Pt (1)/Co (0.7)/Ta (1).

netic layer thickness,  $\hbar$  as the Planck constant,  $j_e$  as the applied current density and  $e$  as the electronic charge. The saturation magnetization,  $M_s=700$  emu/cc, was obtained using alternating gradient force magnetometry (AGFM). We obtained  $\theta_{sh}=0.054$ . It should be noted that planar Hall effect correction was negligible in our stack due to the absence of angular dependence of magnetic field on the harmonic voltages.

To study the effect of Ta capping thickness on the SOT strength, Ta thickness was increased to 3 nm. AC harmonic measurements were performed as before at a current density of  $1.53 \times 10^{11}$  A/m<sup>2</sup>. Fig. 3(a)–(d) show the plots which have the same trend as Fig. 2(a)–(d). Fig. 3(e)–(f) show the linear relationship between  $H_{\text{SL}}$  and  $H_{\text{FL}}$  with the applied current density.  $H_{\text{SL}}$  and  $H_{\text{FL}}$  were evaluated as 49.1 Oe per  $10^{11}$  A/m<sup>2</sup> and 10.9 Oe per  $10^{11}$  A/m<sup>2</sup>, respectively, from the slopes of the plots. The SHA was calculated as 0.15, considering  $M_s=720$  emu/cc. Thus on increasing the thickness three times, the spin Hall angle also increased nearly three times. This is due to the enhancement in spin current injection from the heavy metal Ta layer and hence larger torque on account of higher thickness. The thickness of Ta was limited to 3 nm due to the saturation of spin current density on account of finite spin diffusion length [30,31].

The effect of Pt spacer thickness was investigated by increasing the thickness to 1 nm while keeping the Ta capping thickness as 1 nm. AC harmonics measurements were performed as before at a current density of  $1.96 \times 10^{11}$  A/m<sup>2</sup>. Fig. 4(a)–(d) show the plots, which have the same trend as Fig. 2(a)–(d) with the exception that  $V_{2\omega}$  intersect at lower fields for  $+M_z$  and  $-M_z$  magnetization directions when transverse field is varied.  $H_{\text{SL}}$  and  $H_{\text{FL}}$  were evaluated as 12.8 Oe per  $10^{11}$  A/m<sup>2</sup> and 5.7 Oe per  $10^{11}$  A/m<sup>2</sup>, respectively, from the slopes of the plots. The SHA was calculated as 0.04, considering  $M_s=680$  emu/cc. Increasing the Pt spacer thickness would compensate the SOT from the bottom Pt layer and partially cancel the strength. However, the top ferromagnetic layer would experience some enhancement in the SOT strength. The SHA would depend on the net effect of these torques.

To compute the magnetization switching current density of the devices, an in-plane field of 500 Oe was applied and a quasi-static in-plane current was swept across the wire. A hysteretic magnetic switching between up and down magnetization states was observed with the positive in-plane field favouring down magnetization state at positive current, Fig. 5 shows the comparison of switching current density for the three devices namely, original: Ta (3)/Pt (3)/Co (0.7)/Pt (0.5)/Co (0.7) Ta (1); thick Ta cap: Ta (3)/Pt (3)/Co (0.7)/Pt (0.5)/Co (0.7) Ta (3) and thick Pt spacer: Ta (3)/Pt (3)/Co (0.7)/Pt (1)/Co (0.7) Ta (1). The current density for switching the original device is

$2.8 \times 10^{11}$  A/m<sup>2</sup>, which reduces to  $1.5 \times 10^{11}$  A/m<sup>2</sup> on increasing the Ta capping thickness and rises to  $3.1 \times 10^{11}$  A/m<sup>2</sup> on increasing the Pt spacer thickness. Thus device exhibiting larger effective SOT field and SHA requires lesser current density for switching, making the switching process more efficient.

### 3. Conclusion

In summary, AC harmonic measurements were performed on Co/Pt double stacks to ascertain the effective fields due to SOT and SHA due to the heavy metal layers. The Co/Pt double stack is a modification of the single stack Pt/Co/Ta to enhance the thermal stability and PMA strength. The device exhibited a SHA of 0.05, which rose to 0.15 on increasing the Ta capping thickness three times due to the enhancement in spin current injection efficiency. The SHA reduced to 0.04 on doubling the Pt spacer thickness due to partial cancellation of SOT from the lower Pt layer. The enhancement in SOT also reduced the magnetization switching current density for the corresponding devices thereby making the switching process more energy efficient.

### Competing financial interests

The authors declare no competing financial interest.

### Acknowledgements

This work was supported by the Singapore National Research Foundation, Prime Minister's Office, under a Competitive Research Programme (Non-volatile Magnetic Logic and Memory Integrated Circuit Devices, NRF-CRP9-2011-01), and an Industry-IHL Partnership Program (NRF2015-IIP001-001). The work was also supported by a MOE-Acrf Tier 2 Grant (MOE 2013-T2-2-017). WSL is a member of the Singapore Spintronics Consortium (SG-SPIN).

### References

- [1] S.S.P. Parkin, M. Hayashi, L. Thomas, *Science* 320 (2008) 190–194.
- [2] D.A. Allwood, G. Xiong, C.C. Faulkner, D. Atkinson, D. Petit, R.P. Cowburn, *Science* 309 (2005) 1688–1692.
- [3] C. Murapaka, P. Sethi, S. Goolaup, W.S. Lew, *Sci. Rep.* 6 (2016) 20130.
- [4] P. Sethi, C. Murapaka, S. Goolaup, Y.J. Chen, S.H. Leong, W.S. Lew, *Sci. Rep.* 6 (2016) 19027.
- [5] J.C. Slonczewski, *J. Magn. Magn. Mater.* 159 (1996) L1–L7.
- [6] L. Berger, *Phys. Rev. B* 54 (1996) 9353–9358.
- [7] I.M. Miron, K. Garello, G. Gaudin, P.-J. Zermatten, M.V. Costache, S. Auffret, S. Bandiera, B. Rodmacq, A. Schuhl, A. P. Gambardella, *Nature* 476 (2011) 189–194.
- [8] L. Liu, O.J. Lee, T.J. Gudmundsen, D.C. Ralph, R.A. Buhrman, *Phys. Rev. Lett.* 109 (2012) 096602.
- [9] L. Liu, C.-F. Pai, Y. Li, H.W. Tseng, D.C. Ralph, R.A. Buhrman, *Science* 336 (2012) 555–558.
- [10] I.M. Miron, T. Moore, H. Szabolcs, L.D. Buda-Prejbeanu, S. Auffret, B. Rodmacq, S. Pizzini, J. Vogel, M. Bonfim, A. Schuhl, G. Gaudin, *Nat. Mater.* 10 (2011) 419–423.
- [11] P.P.J. Haazen, E. Mure, J.H. Franken, R. Lavrijssen, H.J.M. Swagten, B. Koopmans, *Nat. Mater.* 12 (2013) 299–303.
- [12] S. Emori, U. Bauer, S.-M. Ahn, E. Martinez, G.S.D. Beach, *Nat. Mater.* 12 (2013) 611–616.
- [13] K.-S. Ryu, L. Thomas, S.-H. Yang, S.S.P. Parkin, *Nat. Nanotechnol.* 8 (2013) 527–533.
- [14] A. Brataas, K.M.D. Hals, *Nat. Nanotechnol.* 9 (2014) 86–88.
- [15] M. Cubukcu, O. Boule, M. Drouard, K. Garello, C.O. Avci, I.M. Miron, J. Langer, B. Ocker, P. Gambardella, G. Gaudin, *Appl. Phys. Lett.* 104 (2014) 042406.
- [16] D. Bhowmik, L. You, S. Salahuddin, *Nat. Nanotech* 9 (2014) 59–63.
- [17] P. Sethi, C. Murapaka, G.J. Lim, W.S. Lew, *Appl. Phys. Lett.* 107 (2015) 192401.
- [18] J. Kim, J. Sinha, M. Hayashi, M. Yamanouchi, S. Fukami, T. Suzuki, S. Mitani, H. Ohno, *Nat. Mater.* 12 (2013) 240–245.
- [19] J. Torrejon, F. Garcia-Sanchez, T. Taniguchi, J. Sinha, S. Mitani, J.-V. Kim, M. Hayashi, *Phys. Rev. B* 91 (2015) 214434.
- [20] C.-F. Pai, L. Liu, Y. Li, H.W. Tseng, D.C. Ralph, R.A. Buhrman, *Appl. Phys. Lett.* 101 (2012) 096602.
- [21] Q. Hao, G. Xiao, *Phys. Rev. Appl.* 3 (2015) 034009.
- [22] X. Fan, J. Wu, Y. Chen, M.J. Jerry, H. Zhang, J.Q. Xiao, *Nat. Commun.* 4 (2013) 1799.
- [23] S. Woo, M. Mann, A.J. Tan, L. Caretta, G.S.D. Beach, *Appl. Phys. Lett.* 105 (2014)

- 212404.
- [24] X. Qiu, K. Narayanapillai, Y. Wu, P. Deorani, D.-H. Yang, W.-S. Noh, J.-H. Park, K.-J. Lee, H.-W. Lee, H. Yang, *Nat. Nanotechnol.* 10 (2015) 333.
- [25] A.W.J.Wells, P.M.Shepley, C.H.Marrows, T.A.Moore, e-print arXiv:1608.03826v1 [cond-mat]
- [26] U.H. Pi, K.W. Kim, J.Y. Bae, S.C. Lee, Y.J. Cho, K.S. Kim, S. Seo, *Appl. Phys. Lett.* 97 (2010) 162507.
- [27] M. Hayashi, J. Kim, M. Yamanouchi, H. Ohno, *Phys. Rev. B* 89 (2014) 144425.
- [28] K. Garello, I.M. Miron, C.O. Avci, F. Freimuth, Y. Mokrousov, S. Blugel, S. Auffret, O. Boulle, G. Gaudin, P. Gambardella, *Nat. Nanotechnol.* 8 (2013) 587–593.
- [29] A.V. Khvalkovskiy, V. Cros, D. Apalkov, V. Nikitin, M. Krounbi, K.A. Zvezdin, A. Anane, J. Grollier, A. Fert, *Phys. Rev. B* 87 (2013) 020402.
- [30] C. Hahn, G. de Loubens, O. Klein, M. Viret, V.V. Naletov, J.B. Youssef, *Phys. Rev. B* 87 (2013) 174417.
- [31] G. Allen, S. Manipatruni, D.E. Nikonov, M. Doczy, I.A. Young, *Phys. Rev. B* 91 (2015) 144412.